Nucleating a Different Coordination in a Crystal under Pressure: A Study of the *B*1-*B*2 Transition in NaCl by Metadynamics

Matej Badin[1,2,*] and Roman Martoňák[2,†]
[1]*SISSA - Scuola Internazionale Superiore di Studi Avanzati, Via Bonomea 265, 34136 Trieste, Italy*
[2]*Department of Experimental Physics, Faculty of Mathematics, Physics and Informatics, Comenius University in Bratislava, Mlynská Dolina F2, 842 48 Bratislava, Slovakia*

(Received 5 May 2021; accepted 21 July 2021; published 31 August 2021)

Here we propose an *NPT* metadynamics simulation scheme for pressure-induced structural phase transitions, using coordination number and volume as collective variables, and apply it to the reconstructive structural transformation *B*1-*B*2 in NaCl. By studying systems with size up to 64 000 atoms we reach a regime beyond collective mechanism and observe transformations proceeding via nucleation and growth. We also reveal the crossover of the transition mechanism from Buerger-like for smaller systems to Watanabe-Tolédano for larger ones. The scheme is likely to be applicable to a broader class of pressure-induced structural transitions, allowing study of complex nucleation effects and bringing simulations closer to realistic conditions.

DOI: 10.1103/PhysRevLett.127.105701

Structural phase transitions in crystals induced by pressure or temperature are complex phenomena of great fundamental and practical importance. Most of them are reconstructive, thermodynamically first order, and involve crossing of free-energy barriers via a nontrivial concerted motion of atoms, representing a rare event. These transitions give rise to a number of important phases with unique properties such as, e.g., diamond created from graphite at high-pressure conditions. In the process of synthesis of such phases, kinetics plays a key role in determining the outcome of the transition, which might not necessarily be the thermodynamically most stable form, but rather a metastable one (e.g., after compression of silicon in the cubic-diamond structure to 11 GPa and decompression to ambient pressure, the BC8 phase is found) [1].

In the past two decades spectacular progress has been made in the prediction of crystalline phases as a result of methods such as evolutionary search [2], random search [3,4], particle swarm optimisation [5], minima hopping [6], etc. These approaches very effectively address the thermodynamics of the problem, identifying stable and metastable structures as global or local minima of the enthalpy surface. However, an understanding of the mechanisms of the transitions, the pertinent barriers in the free-energy surface (FES) and the resulting kinetics still lags behind and more detailed information about the FES is needed to make progress. Commonly used theoretical approaches to uncover possible mechanisms and estimate energetic barrier per unit cell are based on geometric modelling [7–10], group-theory [11–14], phenomenological Landau theory [15], or, more recently, exploration of the FES [16–18]. However, by assuming collective transformation throughout the crystal, they cannot by construction assess the size of the nucleation region and determine the true nucleation barrier. A realistic simulation must therefore reach beyond collective behavior and include nucleation. We note that one of the methods allowing mapping of FES, metadynamics (MetaD) [19] (for recent review see Ref. [20]) was successfully applied to the problem of crystallization from liquid [21–26], which has a number of features similar to those of the problem of solid-solid transitions.

The application of MetaD to structural transitions in crystals started in Refs. [27,28], using the *h*-matrix of the supercell vectors (similarly to the Parrinello-Rahman variable-cell MD [29,30]) as the generic 6D collective variable (CV). This approach is efficient in inducing structural transitions in a number of systems [31–43]; however, the use of a 6D CV essentially limits the use of MetaD to escaping FES minima and precludes the FES reconstruction. For an efficient reconstruction of the FES [44], CVs with dimensionality up to 3 are usually chosen. Moreover, the supercell-based CV by construction works well only for relatively small systems where transitions proceed via collective mechanisms but is unlikely to allow the study of nucleation in a large system. Several approaches addressing an autonomous construction or a choice of CVs have been proposed recently [45–54]. Applications of MetaD to structural transitions not based on the supercell CV are presented in Refs. [55–60].

We present in this Letter a simple and general scheme based on physically motivated CVs such as coordination number (CN) and volume (V) that should be applicable to the important class of pressure-induced structural transitions. This choice is motivated primarily by one of generic rules of high-pressure chemistry formulated by Prewitt and

Downs [61–63] that states that pressure-induced transitions are typically accompanied by an increase of CN in the first coordination sphere. In a more general context, CN was proposed as a reaction coordinate in constrained MD in Ref. [64]. It was also employed in an early MetaD study of a structural transition in carbon [55] and in a MetaD study of the $B1$-$B2$ transition in colloidal clusters [65]. Thermodynamically, in first-order transitions an abrupt densification of the system takes place, with a jump in volume from a few percent up to 10%–20%. We show here that the combination of CN and V appears to provide an effective 2D CV able to drive a pressure-induced structural transition.

We demonstrate the applicability of this scheme on the pressure-induced $B1$-$B2$ transition in NaCl, which represents a paradigmatic but also very complex example of a reconstructive transition [15]. It occurs at room temperature at $p = 26.6$ GPa and involves a volume drop of 5% [66]. Several theoretical collective mechanisms were proposed for this transition, falling essentially into two groups. The ones by Shoji [7], Buerger [8], and Stokes and Hatch [12] are driven mainly by lattice strain while the other class by Hyde and O'Keeffe [9], Watanabe *et al.* (WTM) [10], and Toledáno *et al.* [15] involves more shuffling of atoms [13]. Computational studies include overpressurized variable-cell MD [67,68] and transition path sampling by Zahn and Leoni [69].

We describe NaCl by the well-known and computationally simple Born-Mayer-Huggins-Fumi-Tosi (BMHFT) potential [70,71], which yields for the equilibrium transition pressure at $T = 0$ a value of $p_{\mathrm{eq}} = 19.25$ GPa. Details of the simulation are provided in the Supplemental Material [72].

Structurally, the $B1$-$B2$ transition in NaCl is accompanied by the transfer of two ions with opposite charges from the second to the first coordination shell, increasing the CN from 6 in $B1$ to 8 in $B2$. The average CN between the Na^+ and Cl^- ions can be calculated by means of a switching function as

$$\mathrm{CN} = \frac{2}{N} \sum_{\substack{i \in \mathrm{Na}^+ \\ j \in \mathrm{Cl}^-}} \left(1 + \left(\frac{r_{ij} - d_0}{r_0} \right)^6 \right)^{-1}, \qquad (1)$$

where r_{ij} is the distance between the ith cation and the jth anion and N is the total number of atoms. The choice of the parameters d_0 and r_0 requires some attention. The switching function should allow to clearly differentiate between the initial state (e.g., $B1$), the transition state, and the final state (e.g., $B2$) [20]. Moreover, its slope should be sufficiently high at the positions of the radial distribution function (RDF) peaks of the $B1$ phase corresponding to the first and the second coordination sphere in order to drive an easy exchange of ions between the two spheres. A suitable switching function meeting both requirements is shown in Fig. 1 [79].

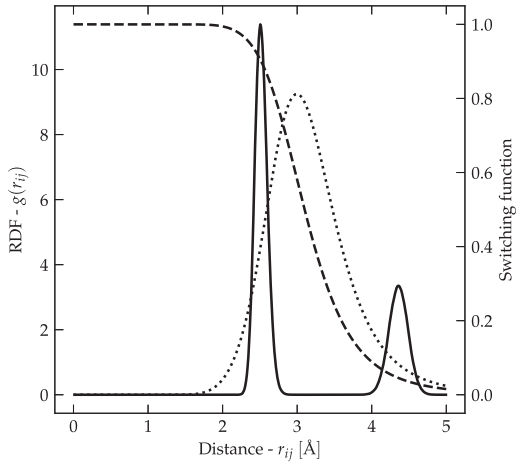

FIG. 1. The Na^+-Cl^- RDF (full) of the $B1$ phase at $p = 20$ GPa and $T = 300$ K, shown together with the switching function employed (dashed) and the absolute value of its derivative (dotted). Note the overlap of the derivative with the first and second coordination spheres. The parameters of the switching function are $d_0 = 1.3$ Å and $r_0 = 2.1$ Å.

For a system in the $B1$ phase with 512 atoms, we performed both MetaD with only CN as well as one with CN and V as CVs. In both versions, both forward and reverse transitions can be seen; see Supplemental Material [72], Figs. S4–S7. However, the character of the CN evolution in the two cases is different. When only the CN is used as CV, even after the first forward and reverse transitions, the system continues to jump between the two phases, indicating that the CN does not have full control over the system. On the other hand, when V is added, the evolution of CN and V after the first transitions becomes much more diffusive. This can be seen in the cross-correlation between CN and V; see Supplemental Material [72], Figs. S8 and S9. We conclude that CN and V thus represent a good choice of CVs. However, the reconstructed FES in Fig. 2 shows that the structural phases are represented as rather long and narrow valleys. The soft direction (SD) represents "breathing" of the crystal preserving the structure, while the perpendicular hard one (HD) represents a direction of structural change. To improve sampling of such a shaped FES, we introduce a rotation of CVs with origin at the equilibrium point $[\overline{CN}, \bar{V}](p, T)$ of $B1$. Deposited Gaussians thus respect the shape of the valleys, being wide in the SD and narrow in the HD. We first rescale CN and V with respect to $B1$ and then rotate them by an orthogonal transformation, whose components are orthonormal eigenvectors of the covariance matrix of the rescaled coordinates. The covariance matrix was obtained from a short 200 ps unbiased NPT MD simulation at given pressure p and temperature T in the $B1$ phase. A detailed description of the approach is provided in the Supplemental Material [72].

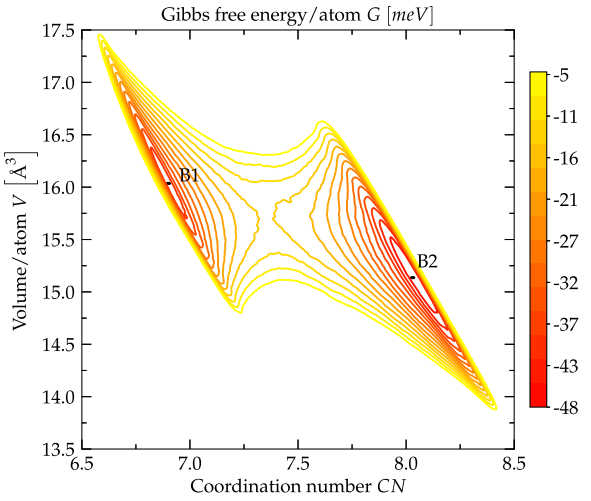

FIG. 2. Reconstructed FES from 100 ns MetaD simulation of a 512-atom system, using CN and V as CVs, at $T = 300$ K and $p = 20$ GPa. Gaussians of height 0.41 meV/atom and width of 0.02 along the CN and 0.02 Å^3 along the volume CV, respectively, were used. The positions of the $B1$ and $B2$ phases are denoted.

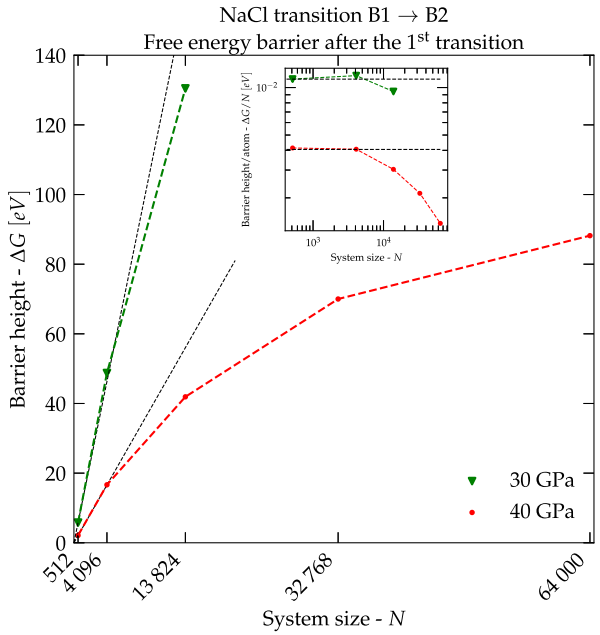

FIG. 3. Barrier heights (from the $B1$ phase) for various system sizes at $T = 300$ K and $p = 30$ and 40 GPa. Straight dotted lines represent the values of the barrier from Buerger collective mechanism. The inset shows the barrier height divided by the system size: $\Delta G/N$ vs the system size N on a log-log plot, highlighting the deviations from the linear scaling characteristic of the collective regime. For larger systems, transformation via nucleation and growth proceeds via a lower barrier than for the collective mechanism.

For illustration, the evolution of the structure of the system across the transition at 40 GPa is shown in the Supplemental Material [72], Fig. S21. The intermediate state (d) is similar to the $B33$ structure that appears in some theoretically proposed mechanisms (see later). It is seen that the whole system first transforms to this transient short-living state, which quickly converts to $B2$, pointing to a collective mechanism of the transition. For some alkali halides, a two-step transition mechanism through the intermediate bulk $B16$ or $B33$ phases was proposed by Toledáno *et al.* [15].

The presented scheme can be readily applied to larger systems, allowing study of precursor effects, nucleation, and growth and access to information about free energy, size, shape, and structure of the critical nucleus. We performed the simulations at $T = 300$ K for various system sizes: $N = 512$, 4096, 13 824, 32 768, and 64 000 atoms. Because the size of the critical nucleus at 20 GPa, close to equilibrium, is expected to be very large, we chose to work at pressures of 30 and 40 GPa. We note that nonclassical nucleation theories (see later) [80] predict also divergence of the size of the critical nucleus on approaching the point of dynamical instability (for our system we found this at 60 GPa).

In Fig. 3 we show the evolution of the transition barrier as a function of system size for two values of pressure [81]. For $p = 30$ GPa the curve appears to grow in a nearly linear manner up to $N = 13\,824$, indicating that even at this moderate overpressurization very large system sizes are necessary to properly accommodate the large critical nucleus. For systems smaller than 4096 atoms, the barrier per atom agrees well with the estimate based on the static Buerger mechanism (see Supplemental Material [72], Fig. S3), showing that the transition proceeds via a collective mechanism. The barrier height in the thermodynamic limit must be larger than 10^2 eV, revealing that homogeneous nucleation in such a regime is physically impossible. At the higher pressure of 40 GPa the curve appears to eventually converge to a value above 90 eV, still too high for a physical transition. Since experimentally the transition at 300 K occurs at $p = 26.6$ GPa [66], it must be assisted by extrinsic factors such as lattice defects [83–87], dislocations [88–95], grain boundaries [96], surfaces [83–85], or nonhydrostatic pressure [97,98]. This observation is similar to the one found for nucleation of melting [94], crystallization of ice [99], and transformation of graphite to diamond [87]. The slow convergence of the barriers can be explained by the presence of long-range ($\sim 1/r^3$) elastic strain fields [83–85,100–102]. We note that the elastic energy of the nucleus and surrounding lattice [83–85,102] is taken into account in nonclassical nucleation theory [80,102–115] but is missing in standard static approaches [7–15] that assume a strictly collective character of the transformation with no interface between the parent and the new phase. It would be fully taken into account in a simulation provided the system is sufficiently large.

We now focus on the structural aspects of the transition. In Fig. 4 we see the critical nucleus (determined as the first

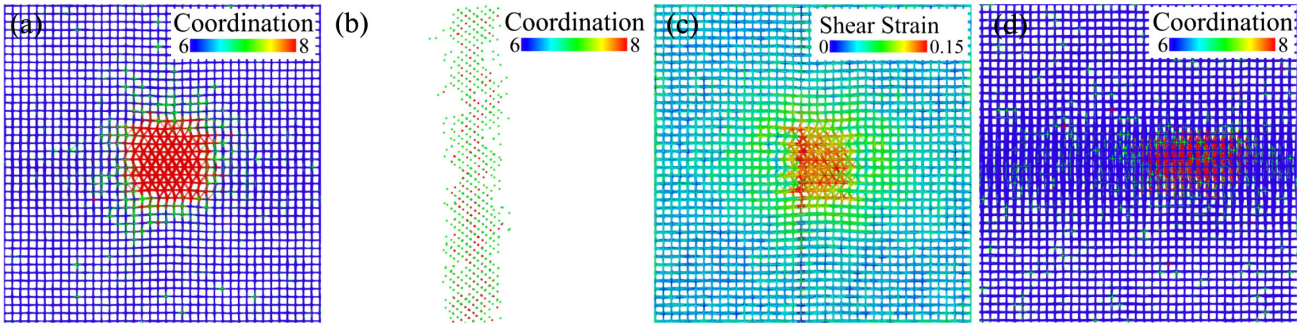

FIG. 4. Critical nucleus of the $B2$ phase (with the shape of a cylinder) in the 64 000-atom system at 40 GPa. (a) Critical nucleus (axis of the cylinder perpendicular to the plane). (b) Perpendicular view of the critical nucleus where only atoms with coordination ≥ 6.5 are shown for clarity. (c) Shear around the critical nucleus in the plane perpendicular to the axis of the cylinder. (d) A localized nucleus with the shape of an ellipsoid (red), 41.7 ps prior to the critical nucleus frame (a). The ellipsoid grows into the cylinder along the axis in which the strain field extends across the PBCs (distortion along horizontal direction). View (d) is perpendicular to both (a) and (b). The pictures were produced using OVITO [116].

time step from which an unbiased MD proceeds toward the $B2$ basin) in the system of 64 000 atoms at 40 GPa. Even at this system size, the critical nucleus represents a cylinder extending across the periodic boundary conditions (PBCs) along one dimension. In all simulations, the nucleus formation starts by creation of strain in a large region of the lattice that extends across the PBCs. In this region the primary nucleus is eventually formed, followed by the creation of a secondary nucleus. At all system sizes and pressures presented, the size of the critical nucleus is not small compared to the system size and PBC artefacts are present. The dependence of shape and size of the critical nucleus on system size and pressure can be found in the Supplemental Material [72].

We further analyzed the detailed transformation mechanism and its dependence on pressure and system size. For convenience, we provide in the Supplemental Material [72] a review of previous results found in the literature. The four idealized collective mechanisms proposed in Ref. [13] can be characterized based on the transformation of the local environment of each atom. $B2$ is formed from $B1$ after addition of two second neighbors of the opposite type to the first coordination shell. All eight of these second neighbors are corners of the conventional `fcc` cell with a given atom in the center. If both these additional second neighbors join at the same time and originally form an edge of the conventional `fcc` cell, one finds the WTM mechanism [10]. On the contrary, if they are located at opposite corners, one finds the Buerger mechanism [8]. Adding the two atoms independently in two steps instead results in the Toledáno [15] (modified WTM) and Stokes and Hatch (modified Buerger) mechanisms, both of which create an intermediate $B33$-like structure [117]. This analysis allows the possibility of different parts of the system transforming at different times via distinct mechanisms. It was performed for all systems considered in the Supplemental Material [72]. The WTM and Toledáno mechanisms are facilitated by the local lattice shear strain, which amounts to a compression along a $\langle 110 \rangle$ direction. This breaks the cubic symmetry and brings four out of eight second neighbors closer to the central atom [see Fig. 5(b)]. It is likely that an application of such uniaxial stress in experiments would reduce hysteresis and facilitate the observation of the transition closer to the thermodynamic transition pressure.

In our simulations, for systems up to 4096 atoms the dominant mechanism is related to the creation of the intermediate (bulk) $B33$ structure that subsequently transforms to $B2$ via the Stokes and Hatch mechanism. For a system size of 4096 atoms, only parts of the system locally transform through the Stokes and Hatch mechanism; see Supplemental Material [72], Fig. S28(e). Finally, for systems larger than 4096 atoms, all atoms within the critical nucleus transform via the Toledáno mechanism. This involves the displacement of planes, as can be seen in Fig. 5(c). In larger systems the Stokes and Hatch mechanism would cost too much energy and therefore nucleation via a zig-zag pattern (WTM or Toledáno mechanism), which causes less strain, appears to be preferable. Nuclei are surrounded by 7-coordinated atoms, but this layer does not resemble $B33$-like structures in large systems.

Our approach is likely to work for a broader class of pressure-induced structural transitions and uncover their microscopic mechanisms in the regime of nucleation and growth, including calculation of free-energy barriers. It might represent a bridge between atomistic modeling of structural phase transitions and effective phase-field theories [80,102–115,118–127]. The use of simple and physically naturally motivated CVs allows a MetaD simulation without prior knowledge of the transition and the final states. This would enhance the predictive value, in particular in cases in which the final state might be either a metastable one or one that is stabilized by entropy and therefore falls beyond the reach of standard $T = 0$ structural prediction methods. It is essential to access long time ($\sim$10 ns) as well as length scales (more than 10^5 atoms), which should be feasible by using machine learning–based

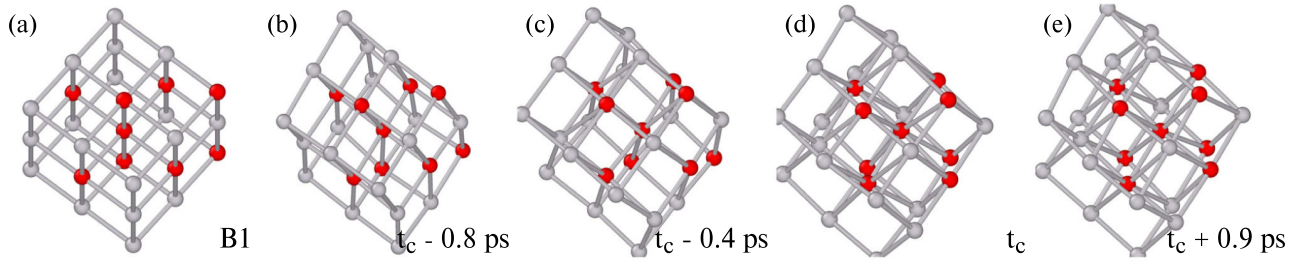

FIG. 5. WTM-like mechanism (Toledáno) observed during the formation and growth of the critical nucleus in the 64 000-atom system at 40 GPa. The central atom and its first and second coordination shell are shown without distinguishing Na and Cl atoms while atoms forming the conventional unit cell of the emerging $B2$ phase are shown in red. All atoms are within the critical nucleus and the cutoff for bonds is set to 3 Å. The position of the central atom and the point of view are fixed. (a) Atoms in the $B1$ lattice. (b)–(e) Atomic configuration at specified times where (d) corresponds to the critical nucleus. The pictures were produced using OVITO [116].

potentials [128–139]. The approach can be generalized to study the role of nonhydrostatic pressure (similarly to Ref. [140]), important in diamond-anvil-cell experiments. Our results point to the need for studying structural transitions in non-idealized environments closer to realistic conditions, including the presence of structural defects, such as dislocations.

We thank G. Bussi, A. Laio, S. Leoni, and C. Molteni for the careful reading of the manuscript and useful comments. R. M. acknowledges stimulating discussions with M. Parrinello, E. Tosatti, A. Laio, and S. Scandolo. M. B. acknowledges all answers to his questions on PLUMED, LAMMPS, and DLPOLY users mailing lists during the course of this work, in particular by G. Bussi and A. M. Elena, as well as funding provided by FMFI UK to attend the NCCR-MARVEL School on VES. This work was supported by the Slovak Research and Development Agency under Contracts No. APVV-15-0496 and No. APVV-19-0371, by VEGA project 1/0640/20, and by Comenius University under Grant for Young Researchers No. UK/436/2021.

*mbadin@sissa.it
†martonak@fmph.uniba.sk

[1] R. H. Wentorf and J. S. Kasper, Science **139**, 338 (1963).
[2] A. R. Oganov and C. W. Glass, J. Chem. Phys. **124**, 244704 (2006).
[3] C. J. Pickard and R. J. Needs, Phys. Rev. Lett. **97**, 045504 (2006).
[4] C. J. Pickard and R. J. Needs, J. Phys. Condens. Matter **23**, 053201 (2011).
[5] Y. Wang, J. Lv, L. Zhu, and Y. Ma, Phys. Rev. B **82**, 094116 (2010).
[6] S. Goedecker, J. Chem. Phys. **120**, 9911 (2004).
[7] H. Shoji, Z. Kristallogr. **77**, 381 (1931).
[8] M. J. Buerger, *Phase Transformations in Solids*, edited by R. Smoluchowski and J. Mayer (John Wiley and Sons, and Hapman Hall Ltd., New York, 1951).
[9] B. Hyde and M. O'Keeffe, in *Phase Transitions*, edited by L. E. Cross (Pergamon, Oxford, 1973), pp. 345–349.
[10] M. Watanabe, M. Tokonami, and N. Morimoto, Acta Crystallogr., Sect. A **33**, 294 (1977).
[11] A. M. Pendás, V. Luaña, J. M. Recio, M. Flórez, E. Francisco, M. A. Blanco, and L. N. Kantorovich, Phys. Rev. B **49**, 3066 (1994).
[12] H. T. Stokes and D. M. Hatch, Phys. Rev. B **65**, 144114 (2002).
[13] H. T. Stokes, D. M. Hatch, J. Dong, and J. P. Lewis, Phys. Rev. B **69**, 174111 (2004).
[14] C. E. Sims, G. D. Barrera, N. L. Allan, and W. C. Mackrodt, Phys. Rev. B **57**, 11164 (1998).
[15] P. Tolédano, K. Knorr, L. Ehm, and W. Depmeier, Phys. Rev. B **67**, 144106 (2003).
[16] C. Shang and Z.-P. Liu, J. Chem. Theory Comput. **9**, 1838 (2013).
[17] S. Maeda, K. Ohno, and K. Morokuma, Phys. Chem. Chem. Phys. **15**, 3683 (2013).
[18] T. Ishikawa, Comput. Mater. Sci. **92**, 36 (2014).
[19] A. Laio and M. Parrinello, Proc. Natl. Acad. Sci. U.S.A. **99**, 12562 (2002).
[20] G. Bussi and A. Laio, Nat. Rev. Phys. **2**, 200 (2020).
[21] H. Niu, P. M. Piaggi, M. Invernizzi, and M. Parrinello, Proc. Natl. Acad. Sci. U.S.A. **115**, 5348 (2018).
[22] P. M. Piaggi and M. Parrinello, J. Chem. Phys. **147**, 114112 (2017).
[23] G. Gobbo, M. A. Bellucci, G. A. Tribello, G. Ciccotti, and B. L. Trout, J. Chem. Theory Comput. **14**, 959 (2018).
[24] P. M. Piaggi and M. Parrinello, Proc. Natl. Acad. Sci. U.S.A. **115**, 10251 (2018).
[25] P. M. Piaggi, O. Valsson, and M. Parrinello, Phys. Rev. Lett. **119**, 015701 (2017).
[26] P. M. Piaggi and M. Parrinello, J. Chem. Phys. **150**, 244119 (2019).
[27] R. Martoňák, A. Laio, and M. Parrinello, Phys. Rev. Lett. **90**, 075503 (2003).
[28] R. Martoňák, D. Donadio, A. R. Oganov, and M. Parrinello, Nat. Mater. **5**, 623 (2006).
[29] M. Parrinello and A. Rahman, Phys. Rev. Lett. **45**, 1196 (1980).
[30] M. Parrinello and A. Rahman, J. Appl. Phys. **52**, 7182 (1981).
[31] R. Martoňák, A. Laio, M. Bernasconi, C. Ceriani, P. Raiteri, F. Zipoli, and M. Parrinello, Z. Kristallogr.—Cryst. Mater. **220**, 489 (2005), https://doi.org/10.1524/zkri.220.5.489.65078.

[32] P. Raiteri, R. Martoňák, and M. Parrinello, Angew. Chem., Int. Ed. **44**, 3769 (2005).
[33] R. Martoňák, D. Donadio, A. R. Oganov, and M. Parrinello, Phys. Rev. B **76**, 014120 (2007).
[34] J. Behler, R. Martoňák, D. Donadio, and M. Parrinello, Phys. Rev. Lett. **100**, 185501 (2008).
[35] C. Bealing, R. Martoňák, and C. Molteni, J. Chem. Phys. **130**, 124712 (2009).
[36] J. Sun, D. D. Klug, and R. Martoňák, J. Chem. Phys. **130**, 194512 (2009).
[37] Y. Yao, D. D. Klug, J. Sun, and R. Martoňák, Phys. Rev. Lett. **103**, 055503 (2009).
[38] J. Sun, D. D. Klug, R. Martoňák, J. A. Montoya, M.-S. Lee, S. Scandolo, and E. Tosatti, Proc. Natl. Acad. Sci. U.S.A. **106**, 6077 (2009).
[39] L. Hromadová and R. Martoňák, Phys. Rev. B **84**, 224108 (2011).
[40] D. Plašienka and R. Martoňák, J. Chem. Phys. **142**, 094505 (2015).
[41] Q. Tong, X. Luo, A. A. Adeleke, P. Gao, Y. Xie, H. Liu, Q. Li, Y. Wang, J. Lv, Y. Yao, and Y. Ma, Phys. Rev. B **103**, 054107 (2021).
[42] R. Martoňák, in *Modern Methods of Crystal Structure Prediction*, edited by A. R. Oganov (Wiley-VCH, Berlin, 2011), pp. 107–130.
[43] R. Martoňák, Eur. Phys. J. B **79**, 241 (2011).
[44] A. Laio, A. Rodriguez-Fortea, F. L. Gervasio, M. Ceccarelli, and M. Parrinello, J. Phys. Chem. B **109**, 6714 (2005).
[45] P. Tiwary and B. J. Berne, Proc. Natl. Acad. Sci. U.S.A. **113**, 2839 (2016).
[46] L. Mones, N. Bernstein, and G. Csányi, J. Chem. Theory Comput. **12**, 5100 (2016).
[47] J. McCarty and M. Parrinello, J. Chem. Phys. **147**, 204109 (2017).
[48] M. M. Sultan and V. S. Pande, J. Chem. Theory Comput. **13**, 2440 (2017).
[49] I. Gimondi, G. A. Tribello, and M. Salvalaglio, J. Chem. Phys. **149**, 104104 (2018).
[50] A. Rodriguez, M. d'Errico, E. Facco, and A. Laio, J. Chem. Theory Comput. **14**, 1206 (2018).
[51] J. Zhang and M. Chen, Phys. Rev. Lett. **121**, 010601 (2018).
[52] M. M. Sultan and V. S. Pande, J. Chem. Phys. **149**, 094106 (2018).
[53] D. Mendels, G. Piccini, Z. F. Brotzakis, Y. I. Yang, and M. Parrinello, J. Chem. Phys. **149**, 194113 (2018).
[54] V. Rizzi, D. Mendels, E. Sicilia, and M. Parrinello, J. Chem. Theory Comput. **15**, 4507 (2019).
[55] F. Zipoli, M. Bernasconi, and R. Martoňák, Eur. Phys. J. B **39**, 41 (2004).
[56] S. Pipolo, M. Salanne, G. Ferlat, S. Klotz, A. M. Saitta, and F. Pietrucci, Phys. Rev. Lett. **119**, 245701 (2017).
[57] I. Gimondi and M. Salvalaglio, J. Chem. Phys. **147**, 114502 (2017).
[58] S. A. Jobbins, S. E. Boulfelfel, and S. Leoni, Faraday Discuss. **211**, 235 (2018).
[59] D. Mendels, J. McCarty, P. M. Piaggi, and M. Parrinello, J. Phys. Chem. C **122**, 1786 (2018).
[60] J. Rogal, E. Schneider, and M. E. Tuckerman, Phys. Rev. Lett. **123**, 245701 (2019).
[61] R. Hemley, *Ultrahigh-Pressure Mineralogy: Physics and Chemistry of the Earth's Deep Interior* (Mineralogical Society of America, Washington, DC, 1998).
[62] W. Grochala, R. Hoffmann, J. Feng, and N. Ashcroft, Angew. Chem., Int. Ed. **46**, 3620 (2007).
[63] M. Miao, Y. Sun, E. Zurek, and H. Lin, Nat. Rev. Chem. **4**, 508 (2020).
[64] M. Sprik, Faraday Discuss. **110**, 437 (1998).
[65] D. Bochicchio, A. Videcoq, and R. Ferrando, J. Chem. Phys. **140**, 024911 (2014).
[66] X. Li and R. Jeanloz, Phys. Rev. B **36**, 474 (1987).
[67] Y. A. Nga and C. K. Ong, Phys. Rev. B **46**, 10547 (1992).
[68] N. Nakagiri and M. Nomura, J. Phys. Soc. Jpn. **51**, 2412 (1982).
[69] D. Zahn and S. Leoni, Phys. Rev. Lett. **92**, 250201 (2004).
[70] F. Fumi and M. Tosi, J. Phys. Chem. Solids **25**, 31 (1964).
[71] M. Tosi and F. Fumi, J. Phys. Chem. Solids **25**, 45 (1964).
[72] See Supplemental Material at http://link.aps.org/supplemental/10.1103/PhysRevLett.127.105701 for a summary of previous studies, details of the simulation technique and detailed account of the simulation results including figures, which includes Refs. [73–78].
[73] J. Anwar, D. Frenkel, and M. G. Noro, J. Chem. Phys. **118**, 728 (2003).
[74] S. Plimpton, J. Comput. Phys. **117**, 1 (1995).
[75] Lammps molecular dynamics simulator.
[76] G. A. Tribello, M. Bonomi, D. Branduardi, C. Camilloni, and G. Bussi, Comput. Phys. Commun. **185**, 604 (2014).
[77] M. Bonomi, G. Bussi, C. Camilloni *et al.*, Nat. Methods **16**, 670 (2019).
[78] G. J. Martyna, D. J. Tobias, and M. L. Klein, J. Chem. Phys. **101**, 4177 (1994).
[79] We note that switching functions appropriately meeting the second requirement change the numerical value of CN in respective phases, e.g. B1, $6 \rightarrow 6.9$, B2, $8 \rightarrow 8.1$. For simplicity, we present true values as such and do not rescale them to neither 6 nor 8.
[80] B. Moran, Y. Chu, and G. Olson, Int. J. Solids Struct. **33**, 1903 (1996).
[81] The barrier height was determined from Gaussians accumulated in MetaD up to the 1st transition. While it is possible to determine it in more accurate manner, e.g. using the well-tempered metadynamics method [82], the accuracy of our simple approach is sufficient for the purpose of our study.
[82] A. Barducci, G. Bussi, and M. Parrinello, Phys. Rev. Lett. **100**, 020603 (2008).
[83] K. C. Russell, Adv. Colloid Interface Sci. **13**, 205 (1980).
[84] *Phase Transformations in Materials*, edited by G. Kostorz (Wiley, New York, 2001).
[85] B. Fultz, *Phase Transitions in Materials* (Cambridge University Press, Cambridge, England, 2020).
[86] P. C. Clapp, Physica (Amsterdam) **66D**, 26 (1993).
[87] R. Z. Khaliullin, H. Eshet, T. D. Kühne, J. Behler, and M. Parrinello, Nat. Mater. **10**, 693 (2011).
[88] J. W. Cahn, Acta Metall. **5**, 169 (1957).
[89] H. Cook, Acta Metall. **21**, 1431 (1973).
[90] G. B. Olson and M. Cohen, Metall. Trans. A **7**, 1897 (1976).

[91] G. B. Olson and M. Cohen, Metall. Trans. A **7**, 1905 (1976).
[92] M. Suezawa and H. Cook, Acta Metall. **28**, 423 (1980).
[93] B. Li, X. M. Zhang, P. C. Clapp, and J. A. Rifkin, J. Appl. Phys. **95**, 1698 (2004).
[94] A. Samanta, M. E. Tuckerman, T.-Q. Yu, and W. E, Science **346**, 729 (2014).
[95] V. I. Levitas, H. Chen, and L. Xiong, in *Proceedings of the International Conference on Martensitic Transformations: Chicago* (Springer International Publishing, New York, 2018), pp. 83–87.
[96] G. B. Olson and M. Cohen, Metall. Trans. A **7**, 1915 (1976).
[97] S. Paul, K. Momeni, and V. I. Levitas, Carbon **167**, 140 (2020).
[98] Y. Gao, Y. Ma, Q. An, V. Levitas, Y. Zhang, B. Feng, J. Chaudhuri, and W. A. Goddard, Carbon **146**, 364 (2019).
[99] E. Sanz, C. Vega, J. R. Espinosa, R. Caballero-Bernal, J. L. F. Abascal, and C. Valeriani, J. Am. Chem. Soc. **135**, 15008 (2013).
[100] F. R. N. Nabarro, Proc. R. Soc. A **175**, 519 (1940).
[101] J. D. Eshelby, Proc. R. Soc. A **241**, 376 (1957).
[102] G. B. Olson and M. Cohen, Le J. Phys. Colloq. **43**, C4 (1982).
[103] P. C. Clapp, Phys. Status Solidi (b) **57**, 561 (1973).
[104] P. C. Clapp, Mater. Sci. Eng. **38**, 193 (1979).
[105] G. Guénin and P. F. Gobin, Metall. Trans. A **13**, 1127 (1982).
[106] R. J. Gooding and J. A. Krumhansl, Phys. Rev. B **39**, 1535 (1989).
[107] F. Falk and P. Konopka, J. Phys. Condens. Matter **2**, 61 (1990).
[108] J. Krumhansl, Solid State Commun. **84**, 251 (1992).
[109] Y. Wang and A. Khachaturyan, Acta Mater. **45**, 759 (1997).
[110] A. Roy, J. M. Rickman, J. D. Gunton, and K. R. Elder, Phys. Rev. E **57**, 2610 (1998).
[111] A. C. Reid, G. B. Olson, and B. Moran, Phase Transitions **69**, 309 (1999).
[112] Y. A. Chu, B. Moran, G. B. Olson, and A. C. E. Reid, Metall. Mater. Trans. A **31**, 1321 (2000).
[113] C. Shen, J. Li, and Y. Wang, Metall. Mater. Trans. A **39**, 976 (2008).
[114] T. W. Heo and L.-Q. Chen, JOM **66**, 1520 (2014).
[115] L. Zhang, W. Ren, A. Samanta, and Q. Du, npj Comput. Mater. **2**, 16003 (2016).
[116] A. Stukowski, Model. Simul. Mater. Sci. Eng. **18**, 015012 (2010).
[117] The detailed description of the algorithm determining the transformation mechanism of the environment of each atom is in Supplemental Material [72]. It is also necessary to distinguish between the mechanism involved in the initial creation of the critical nucleus and the one of the subsequent growth.
[118] V. I. Levitas and D. L. Preston, Phys. Rev. B **66**, 134206 (2002).
[119] V. I. Levitas and D. L. Preston, Phys. Rev. B **66**, 134207 (2002).
[120] V. I. Levitas, D. L. Preston, and D.-W. Lee, Phys. Rev. B **68**, 134201 (2003).
[121] L. Zhang, L.-Q. Chen, and Q. Du, Phys. Rev. Lett. **98**, 265703 (2007).
[122] H. She, Y. Liu, and B. Wang, Int. J. Solids Struct. **50**, 1187 (2013).
[123] V. I. Levitas, J. Mech. Phys. Solids **70**, 154 (2014).
[124] V. I. Levitas and J. A. Warren, J. Mech. Phys. Solids **91**, 94 (2016).
[125] V. I. Levitas, H. Chen, and L. Xiong, Phys. Rev. B **96**, 054118 (2017).
[126] H. Babaei and V. I. Levitas, Int. J. Plast. **107**, 223 (2018).
[127] V. I. Levitas, Int. J. Plast. **106**, 164 (2018).
[128] F. Noé, A. Tkatchenko, K.-R. Müller, and C. Clementi, Annu. Rev. Phys. Chem. **71**, 361 (2020).
[129] J. Behler and M. Parrinello, Phys. Rev. Lett. **98**, 146401 (2007).
[130] C. M. Handley and J. Behler, Eur. Phys. J. B **87**, 152 (2014).
[131] A. Singraber, J. Behler, and C. Dellago, J. Chem. Theory Comput. **15**, 1827 (2019).
[132] J. Behler, Chem. Rev. **121**, 10037 (2021).
[133] L. Zhang, J. Han, H. Wang, R. Car, and W. E, Phys. Rev. Lett. **120**, 143001 (2018).
[134] L. Zhang, J. Han, H. Wang, R. Car, and W. E, J. Chem. Phys. **149**, 034101 (2018).
[135] L. Zhang, D.-Y. Lin, H. Wang, R. Car, and W. E, Phys. Rev. Mater. **3**, 023804 (2019).
[136] S. T. John and G. Csányi, J. Phys. Chem. B **121**, 10934 (2017).
[137] A. P. Bartók, M. C. Payne, R. Kondor, and G. Csányi, Phys. Rev. Lett. **104**, 136403 (2010).
[138] S. Chmiela, H. E. Sauceda, K.-R. Müller, and A. Tkatchenko, Nat. Commun. **9**, 3887 (2018).
[139] Y. Shaidu, E. Küçükbenli, R. Lot, F. Pellegrini, E. Kaxiras, and S. de Gironcoli, npj Comput. Mater. **7**, 52 (2021).
[140] D. Donadio, R. Martoňák, P. Raiteri, and M. Parrinello, Phys. Rev. Lett. **100**, 165502 (2008).